SEEDING OF GÖRTLER VORTICES THROUGH A SUCTION AND BLOWING STRIP

Leandro F. de Souza
Instituto Tecnológico de Aeronáutica
Pç Mal. Eduardo Gomes, 50 - São José dos Campos, SP - 12228 900, Brazil
lefraso@zipmail.com.br

Márcio T. Mendonça
Centro Técnico Aeroespacial, Instituto de Aeronáutica e Espaço
Pç Mal. Eduardo Gomes, 50 - São José dos Campos, SP - 12228 904, Brazil
marcio_tm@yahoo.com

Marcello A. Faraco de Medeiros
USP - Universidade de São Paulo
Escola de Engenharia de São Carlos - Departamento de Engenharia Aeronáutica
Av. Trabalhador São Carlense, 400 - SP - 13566-590, Brazil
marcello@sc.usp.br

Markus Kloker
Institut für Aerodynamik und Gasdynamik - Universität Stuttgart
Stuttgart, Germany
kloker@iag.uni-stuttgart.de

Abstract. *Due to centrifugal instability, the boundary layer over a concave plate produces counter rotating vortices known as Görtler vortices. The resulting wavelength of these vortices are determined, in experimental facilities, by the upstream history of the flow. In isotropic disturbance conditions, the predominant wavelength corresponds to the fastest growing vortices predicted by the linear stability theory. Previous investigations considered the wavelength selection mechanism due to free-stream conditions and wall roughness. The present investigation considers the excitation of Görtler vortices through a suction and blowing strip. The study is based on numerical simulations of the vorticity transport equations derived from the Navier-Stokes equations, written in a curvilinear coordinate system. The resulting vorticity-velocity equations are solved using a compact high-order finite difference technique. The results show that, when the vortices are excited by suction and blowing variation in the spanwise direction according to a cosine function, the first harmonic may have a stronger growth rate then predicted by the weakly nonlinear theory if its wavenumber corresponds to a higher linear stability growth rate. Curves of energy variation for different harmonics and isolines of streamwise velocity in the plane perpendicular to the streamwise direction are presented, showing the dominant mode and the development of the characteristic mushroom structures.*

Key words: *Boundary layer stability, Compact finite difference scheme, Vorticity-velocity formulation, Hydrodynamic instability, Laminar flow transition.*

1. Introduction

In general, turbulent flows are the most common in practical applications. Nevertheless, there are a large number of situations in which transition to turbulence is of significant importance. For example, in the flow over low Reynolds number turbine blades and laminar flow airfoils. The understanding of how transition takes place can help in predicting and even controlling transition to turbulence. Over recent years the body of knowledge on laminar flow stability and transition has increased dramatically due to the development of new experimental and numerical techniques as well as due to advances in applied mathematical theories. Nevertheless, there are many transition scenarios for which a physical explanation is still unknown, and predicting transition location is still a challenge in many engineering applications.

The study of boundary-layer stability over concave surfaces, started by Görtler (1940), has attracted the attention of several scientists. The centrifugal instability mechanism is responsible for the development of counter-rotating vortices, aligned in the streamwise direction, known as Görtler Vortices (GV). Initially these vortices have a very weak growth rate and the resulting wavenumber is strongly dependent on the previous history of the flow. It is therefore easy to create a flow structure with a wavelength different from the fastest growing one.

Bippes (1978) studied experimentally the flow over concave surfaces and presented results for three different upstream conditions: without any disturbance generator, with screens to produce isotropic disturbances and with heated wires in order to have controlled disturbances. In all the experiments he found the characteristic counter-rotating vortices. When using screens, Bippes suggests that the selected wavelength follows the maximum amplification curve predicted by linear stability theory (LST).

A well documented article presenting experimental results was written by Swearingen and Blackwelder (1987). Their results are frequently used for validation by numerical experimentalists. They said that the repeatability of the experiments was very good although they did not use any mechanism to generate disturbances. The resulting spanwise pattern was found to depend on the last screen chamber used to control the turbulence level. Myose and Blackwelder (1991) show results where the GV wavelength was changed by varying the amount of tunnel side wall boundary layer removal just upstream of the concave wall test section leading edge. They concluded that when the disturbance field is isotropic the wavenumber along the largest amplification curve is the preferred one.

Hall (1982) presented a parabolic model for the development of GV, questioning the formulation based on normal modes of a parallel base flow. He states that the vortices depend on the previous history of the flow and that the resulting growth rate is dependent on the initial disturbance and on its initial location. Lee and Liu (1992) reproduced numerically the experimental study of Swearingen and Blackwelder with a parabolic model. They used eigenfunctions obtained from local normal mode analysis as initial conditions. They found the same growth rate while initiating the simulations in three different streamwise positions. They concluded that different initial disturbances tend to GV predicted by a normal mode analysis further downstream. They attributed the results obtained by Hall to the use of not necessarily hydrodynamic possible initial conditions. With their formulations, Lee and Liu were successful in obtaining the mushroom shape structures, that are characteristic of GV.

Guo and Finlay (1994) studied the wavenumber selection, splitting and merging of Dean and Görtler Vortices. They showed that when the energy level of GV is low, the spatial growth of the vortices is governed by primary instability. At this stage, vortices with different wavelength can develop at the same time and show no significant interaction with each other. They also found that for large wavenumbers a new pair of vortices with different wavelength is likely to appear, causing a splitting of the original vortices.

Recognizing that in experimental apparatus the GV are seeded by either upstream screens and wall roughness, Bottaro and Zebib (1997) studied different wall roughness distributions and their influence in GV formation. They found the preferable wavelength to be near the most amplified one for different disturbance inducers. They also found that triangular riblets are the best GV promoters, but in this case the wavelength is set by the distance between the riblets and not by the mode with the largest amplification rate. They also found that before the instability mechanism can start to amplify disturbances, there is a linear filtering region, which they called receptivity region.

As can be concluded from all these investigations, several techniques can be used to 'seed' Görtler vortices in the flow field in experimental facilities and numerical simulations. Previous investigations considered the wavelength selection mechanism due to free-stream conditions and wall roughness, in this study the perturbation is introduced by suction and blowing at the wall in a region called disturbance strip. The normal velocity component at the wall varies with a cosine function in the spanwise direction. It is shown that there exists a region between the disturbance strip and the region where these disturbances propagates as classic GV. In this region, which we called receptivity region, perturbations are filtered by the boundary layer. Tests were made in order to verify the behavior of the flow in the receptivity region and in the following GV dominated region. The study is performed using spatial Direct Numerical Simulation (DNS).

The paper is structured in the following way: first the formulation and the numerical method are presented, including a discussion about the types of boundary conditions and damping zones used near boundaries to avoid wave reflections; then verification and validation test cases are presented comparing the DNS results with results from other numerical models (Mendonça, 2000; Lee and Liu, 1992; Li and Malik, 1995) and with experimental results from Swearingen and Blackwelder (1987); next the disturbance behavior in the receptivity region downstream of the suction-blowing zone is analyzed for different spanwise wavenumbers and the last part presents the conclusions and final comments.

2. Formulation

In this study, the governing equations are the incompressible, unsteady Navier-Stokes equations with constant density and viscosity. They consist of the momentum equations for the velocity components (u, v, w) in the streamwise direction (x), wall normal direction (y) and spanwise direction (z):

$$\frac{\partial u}{\partial t} + u\frac{\partial u}{\partial x} + v\frac{\partial u}{\partial y} + w\frac{\partial u}{\partial z} = -\frac{\partial p}{\partial x} + \nabla^2 u, \tag{1}$$

$$\frac{\partial v}{\partial t} + u\frac{\partial v}{\partial x} + v\frac{\partial v}{\partial y} + w\frac{\partial v}{\partial z} + \frac{Go^2(u^2)}{\sqrt{Re}h} = -\frac{\partial p}{\partial y} + \nabla^2 v, \tag{2}$$

$$\frac{\partial w}{\partial t} + u\frac{\partial w}{\partial x} + v\frac{\partial w}{\partial y} + w\frac{\partial w}{\partial z} = -\frac{\partial p}{\partial z} + \nabla^2 w, \tag{3}$$

and the continuity equation:

$$\frac{\partial u}{\partial x} + \frac{\partial v}{\partial y} + \frac{\partial w}{\partial z} = 0, \tag{4}$$

where p is the pressure and $\nabla^2 = \frac{1}{Re}\left(\frac{\partial^2}{\partial x^2} + \frac{\partial^2}{\partial y^2} + \frac{\partial^2}{\partial z^2}\right)$.

The variables used in the above equations are non-dimensional. They are related to the dimensional variables by:

$$x = \frac{\bar{x}}{\bar{L}}, \quad y = \frac{\bar{y}}{\bar{L}}, \quad z = \frac{\bar{z}}{\bar{L}}, \quad k_c = \frac{\bar{L}}{\bar{R}}, \quad u = \frac{\bar{u}}{\bar{U}_\infty},$$

$$v = \frac{\bar{v}}{\bar{U}_\infty}, \quad w = \frac{\bar{w}}{\bar{U}_\infty}, \quad t = \frac{\bar{t}\bar{U}_\infty}{\bar{L}}, \quad Re = \frac{\bar{U}_\infty \bar{L}}{\bar{\nu}}, \tag{5}$$

where Re is the Reynolds number, the terms with an over-bar are dimensional terms, $\bar{L}$ is the reference length, $\bar{U}_\infty$ is the free-stream velocity, $\bar{\nu}$ is the kinematic viscosity and $\bar{R}$ is the radius of curvature.

The Görtler number is given by $Go = (k_c\sqrt{Re})^{1/2}$. In these equations, the term $(Go^2u^2)/(\sqrt{Re}h)$ is the leading order curvature term, where $h = 1 - k_c y$ and k_c is the curvature of the wall.

The vorticity here is defined as the negative curl of velocity vector. Knowing that and taking the negative curl of the momentum equations (1) to (3) and using the fact that both the velocity and the vorticity vectors are solenoidal, one can obtain the vorticity transport equation in each direction:

$$\frac{\partial \omega_x}{\partial t} + \frac{\partial a}{\partial y} - \frac{\partial b}{\partial z} + \frac{Go^2}{\sqrt{Re}h}\frac{\partial (u^2)}{\partial z} = \nabla^2 \omega_x, \tag{6}$$

$$\frac{\partial \omega_y}{\partial t} + \frac{\partial c}{\partial z} - \frac{\partial a}{\partial x} = \nabla^2 \omega_y, \tag{7}$$

$$\frac{\partial \omega_z}{\partial t} + \frac{\partial b}{\partial x} - \frac{\partial c}{\partial y} - \frac{Go^2}{\sqrt{Re}h}\frac{\partial (u^2)}{\partial x} = \nabla^2 \omega_z, \tag{8}$$

where $a = v\omega_x - u\omega_y$, $b = u\omega_z - w\omega_x$ and $c = w\omega_y - v\omega_z$ are the nonlinear terms resulting from convection, vortex stretching and vortex bending.

Taking the definition of the vorticity and the mass conservation equation, one can obtain a Poisson equation for each velocity component:

$$\frac{\partial^2 u}{\partial x^2} + \frac{\partial^2 u}{\partial z^2} = -\frac{\partial \omega_y}{\partial z} - \frac{\partial^2 v}{\partial x \partial y}, \tag{9}$$

$$\frac{\partial^2 v}{\partial x^2} + \frac{\partial^2 v}{\partial y^2} + \frac{\partial^2 v}{\partial z^2} = -\frac{\partial \omega_z}{\partial x} + \frac{\partial \omega_x}{\partial z}, \tag{10}$$

$$\frac{\partial^2 w}{\partial x^2} + \frac{\partial^2 w}{\partial z^2} = \frac{\partial \omega_y}{\partial x} - \frac{\partial^2 v}{\partial y \partial z}. \tag{11}$$

The flow is assumed to be periodic and symmetric with respect to $z = 0$ in the spanwise (z) direction. Therefore, the flow field is expanded in real Fourier cosine and sine series with K spanwise Fourier modes:

$$(u, v, \omega_z, b, c) = \sum_{k=0}^{K} (U_k, V_k, \Omega_{z_k}, B_k, C_k)\cos(\beta_k z) \qquad (w, \omega_x, \omega_y, a) = \sum_{k=1}^{K} (W_k, \Omega_{x_k}, \Omega_{y_k}, A_k)\sin(\beta_k z) \tag{12}$$

where β_k is the spanwise wavenumber given by $\beta_k = 2\pi k/\lambda_z$, and λ_z is the spanwise wavelength of the fundamental spanwise Fourier mode.

Substituting the cosine and sine transforms (Eq. 12) in the vorticity transport equations (6 to 8) and in the velocity Poisson equations (9 to 11) yields the governing equations in the Fourier space:

$$\frac{\partial \Omega_{x_k}}{\partial t} + \frac{\partial A_k}{\partial y} - \beta_k B_k - \frac{Go^2}{\sqrt{Re}}\frac{\beta_k (U_k^2)}{h} = \nabla_k^2 \Omega_x, \tag{13}$$

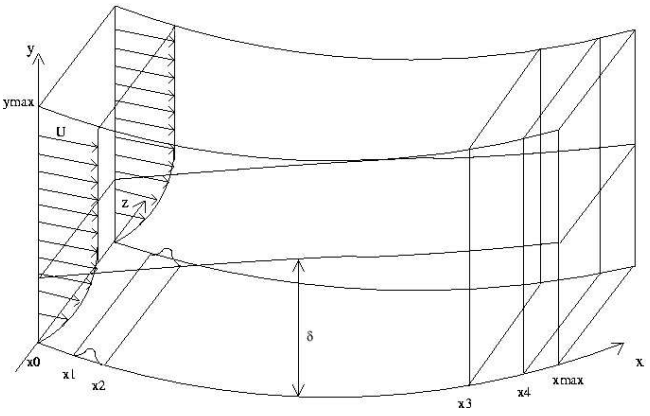

Figure 1: Integration domain.

$$\frac{\partial \Omega_{y_k}}{\partial t} + \beta_k C_k - \frac{\partial A_k}{\partial x} = \nabla_k^2 \Omega_y, \tag{14}$$

$$\frac{\partial \Omega_{z_k}}{\partial t} + \frac{\partial B_k}{\partial x} + \frac{\partial C_k}{\partial y} - \frac{Go^2}{\sqrt{Re}h}\frac{\partial (U_k^2)}{\partial x} = \nabla_k^2 \Omega_z, \tag{15}$$

$$\frac{\partial^2 U_k}{\partial x^2} - \beta_k^2 U_k = -\beta_k \Omega_{y_k} - \frac{\partial^2 V_k}{\partial x \partial y}, \tag{16}$$

$$\frac{\partial^2 V_k}{\partial x^2} + \frac{\partial^2 V_k}{\partial y^2} - \beta_k^2 V_k = -\frac{\partial \Omega_{z_k}}{\partial x} + \beta_k \Omega_{x_k}, \tag{17}$$

$$\frac{\partial^2 W_k}{\partial x^2} - \beta_k^2 W_k = \frac{\partial \Omega_{y_k}}{\partial x} + \beta_k \frac{\partial V_k}{\partial y}, \tag{18}$$

where $\nabla_k^2 = \frac{1}{Re}\left(\frac{\partial^2}{\partial x^2} + \frac{\partial^2}{\partial y^2} - \beta_k^2\right)$.

The governing equations are complemented by the specification of boundary conditions. At the wall no-slip and no penetration conditions are imposed, except at the suction and blowing region where the wall-normal velocity component is specified. At the inflow the velocity and vorticity components are specified based on the Blasius boundary layer solution. At the upper boundary the vorticity disturbances decay exponentially to zero. Finally, at the outflow boundary the second derivative of all dependent variables are set to zero.

3. Numerical Method

The Eqs.(13) to (18) are solved numerically inside the integration domain shown schematically in Fig. 1. The calculation are done on a orthogonal uniform grid, parallel to the wall. The fluid enters the computational domain at $x = x_0$ and exits at the outflow boundary $x = x_{max}$. Disturbances are introduced into the flow field using a suction and blowing function at the wall in a disturbance strip. This region is located between x_1 and x_2. In the region located between x_3 and x_4 a buffer domain technique was implemented in order to avoid wave reflections at the outflow boundary. In these simulations a Blasius boundary layer is used as the base flow.

At the inflow boundary ($x = x_0$), all velocity and vorticity components are specified. At the outflow boundary ($x = x_{max}$), the second derivative of the velocity and vorticity components in the streamwise direction are set to zero. At the upper boundary ($y = y_{max}$) the flow is assumed to be irrotational. This is satisfied by setting all vorticity and their derivatives to zero. An exponential decay of the velocity is imposed using the condition:

$$\frac{\partial V_k}{\partial y}|_{x,y_{max},t} = -\frac{\beta_k}{\sqrt{Re}} V_k(x, y_{max}, t). \tag{19}$$

At the wall ($y = 0$), no-slip conditions are imposed for the streamwise (U_k) and the spanwise (W_k) velocity components. For the wall-normal velocity component (V_k) the non-permeability and no-penetration conditions are imposed in all points at the wall except between x_1 and x_2, where the disturbances are introduced. In addition, the condition $\partial V_k/\partial y = 0$ is imposed to ensure conservation of mass. The equations used for evaluating the vorticity components at the wall are:

$$\frac{\partial^2 \Omega_{x_k}}{\partial x^2} - \beta_k^2 \Omega_{x_k} = -\frac{\partial^2 \Omega_{y_k}}{\partial x \partial y} - \beta_k \nabla_k^2 V_k \quad \text{and} \quad \frac{\partial \Omega_{z_k}}{\partial x} = \beta_k \Omega_{x_k} - \nabla_k^2 V_k. \tag{20}$$

The introduction of the disturbances at the wall is done via a slot in the region ($i_1 \leq i \leq i_2$), where i_1 and i_2 are, respectively, the first and the last point of the disturbance strip, in the x direction. The function used for the variation of the normal velocity V_k along the streamwise direction is:

$$V_k(i,0,t) = A\sin^3(\epsilon) \quad \text{for} \quad i_1 \leq i \leq i_2 \quad \text{and} \quad V_k(x,0,t) = 0 \quad \text{for} \quad i < i_1 \quad \text{and} \quad i > i_2, \tag{21}$$

where $\epsilon = \pi(i - i_1)/(i_2 - i_1)$ and A is a real constant that can be chosen to adjust the amplitude of the disturbance. The chosen function ($\sin^3$) ensures that, at $i = i_1$ and $i = i_2$, the normal velocity component, its first derivatives and second do not have a discontinuity going in and out of the disturbance strip region. The variable i indicates the grid point location x_i in the streamwise direction, and points i_1 and i_2 correspond to x_1 and x_2 respectively.

A damping zone near the outflow boundary is defined in which all the disturbances are gradually damped down to zero. This technique is well documented in Kloker et al. (1993), where the advantages and requirements are discussed. In the work of Meitz and Fasel (2000), they adopted a fifth order polynomium, and the same function was used in the present simulations. The basic idea is to multiply the vorticity components by a ramp function $f_2(x)$ after each step of the integration method. This technique has proved to be very efficient in avoiding reflections that could come from the outflow boundary conditions when simulating disturbed flows. Using this technique, the vorticity components are taken as:

$$\Omega_k(x,y) = f_2(x)\Omega_k(x,y,t), \tag{22}$$

where $\Omega_k(x,y,t)$ is the disturbance vorticity component that comes out from the Runge-Kutta integration and $f_2(x)$ is a ramp function that goes smoothly from 1 to 0.

The implemented function was:

$$f_2(x) = f(\epsilon) = 1 - 6\epsilon^5 + 15\epsilon^4 - 10\epsilon^3, \tag{23}$$

where $\epsilon = (i - i_3)/(i_4 - i_3)$ for $i_3 \leq i \leq i_4$. The points i_3 and i_4 correspond to the positions x_3 and x_4 in the streamwise direction respectively. To ensure good numerical results a minimum distance between x_3 and x_4 and between x_4 and the end of the domain - x_{max} should be specified. The zones in the simulations presented here has 30 grid points in each region.

Another buffer domain, located near the inflow boundary is also implemented in the code. As pointed out by Meitz (1996), in simulations involving streamwise vortices, reflections due to the vortices at the inflow can cause difficulties. The function adopted here is similar to the one used for the outflow boundary:

$$f_3(x) = f(\epsilon) = 6\epsilon^5 - 15\epsilon^4 + 10\epsilon^3, \tag{24}$$

where ϵ is $\epsilon = (i - 1)/(i1 - 1)$ for the range $1 \leq i \leq i_1$. All the vorticity components are multiplied by this function in this region.

Simulations with two different types of buffer domain were carried out. In the first type, the function given in Eq.(24) was applied to all Fourier modes between x_0 and x_1. In the second type, the damping function was used only for the fundamental Fourier mode in the region between x_0 and x_1. For the other Fourier modes, all the vorticity components are set to zero between x_0 and x_2. The damping function is used between x_2 and $2 \times x_2$ for all modes but the fundamental. The reasons and advantages of these two techniques are discussed in Sec. 4.

The time derivatives in the vorticity transport equations were discretized with a classical 4^{th} order Runge-Kutta integration scheme (Ferziger and Peric, 1997). The steps 4 to 9 were carried out for each step of the Runge-Kutta method. The spatial derivatives were calculated using a 6^{th} order compact finite difference scheme (Souza et al., 2002a; Souza et al., 2002b). The differences between the scheme used in this work and the approximations shown by Lele (1992) are in the discretization of the boundary and near boundary points. At the boundaries, a 3^{rd} order approximation is proposed by Lele, whereas for points near the boundaries he proposed a 4^{th} order approximation. In the current work a 5^{th} order approximation for the boundary points was adopted, while for points near the boundaries, a 6^{th} order approximation was used. More details of this compact scheme can be found in Souza et al. (2002a). The V-Poisson equation (17) was solved using a Full Approximation Scheme (FAS) multigrid (Trottenberg and Hackbusch, 1986). A v-cycle working with 4 grids was implemented.

4. Numerical Results

4.1. Validation

In order to test the accuracy and reliability of the mathematical model and of the numerical implementation some tests were performed. The results obtained with the current code were compared with results obtained

with different models (Mendonça, 2000; Li and Malik, 1995; Lee and Liu, 1992) and experimental results (Swearingen and Blackwelder, 1987).

The parameters used in the test case were those from the experiment of Swearingen and Blackwelder (1987) who considered a boundary layer on a concave plate with $\overline{R} = 3.20$ m. The free-stream velocity is $\overline{U}_\infty = 5$ m/s. The simulation starts at $x_0 = 10$ cm from the leading edge, which corresponds to a boundary-layer thickness parameter $\delta = \sqrt{\bar{\nu}\bar{x}_0/\bar{U}_\infty} = 5.477$ cm, a Görtler number $Go = 2.38859$, and a Reynolds number $Re = 33124$. The average spanwise wavelength was $\bar{\lambda}_z = 1.8$ cm in the experiment, which corresponds to a non-dimensional wavenumber of $\beta = 34.90$. This corresponds to a wavelength parameter for the fundamental Fourier mode, given by $\Lambda_f = (\bar{U}_\infty \bar{\lambda}_z/\bar{\nu})(\bar{\lambda}_z/\bar{R})^{1/2}$, of $\Lambda_f = 450$. The reference length used was $\bar{L} = 10$ cm. The number of points used was 321 and 281 in the streamwise and the wall-normal directions respectively. The grid spacing was 0.04 and 8.25×10^{-4} in the streamwise and the wall-normal directions respectively. The disturbance-strip location was $1.6 \leq x \leq 2.6$. The number of Fourier modes simulated was 7. The buffer-domain technique adopted near the inflow was of the second type. Test runs with a smaller grid spacing and larger number of Fourier modes indicated that the solutions were grid independent.

Figure 2 - left presents the streamwise development of the energy in each k Fourier mode. The energy is defined as:

$$E_k = \int_0^\infty \left(|u_k'|^2 + |v_k'|^2 + |w_k'|^2\right) dy \quad \text{if} \quad k > 0 \quad \text{and} \quad E_k = \frac{1}{2}\int_0^\infty \left(|u_k'|^2 + |w_k'|^2\right) dy \quad \text{for} \quad k = 0. \quad (25)$$

The energy of the mean flow distortion did not take into account the velocity component normal to the wall v_0' to allow comparisons with the PSE model, where v_0' does not go to zero as $y \to \infty$. The ($'$) symbol indicates that only the disturbances are taken into account.

Another verification test case compares DNS results, PSE results (Mendonça, 2000) and numerical results from Li and Malik (1995). All the flow conditions were identical to those in the experimental arrangement of Swearingen and Blackwelder, but the wavenumber was reduced by a factor of 2. The resulting vortices were closer spaced than the most amplified vortex modes given by the LST. Fig. 2 - right shows the streamwise development of the energy for each Fourier. The comparisons show very good agreement between the DNS results and other numerical models. The results obtained with the present model before $x = 40$ cm, correspond to a receptivity region. The available PSE model (Mendonça, 2000) can not go into the region where the nonlinear products are high.

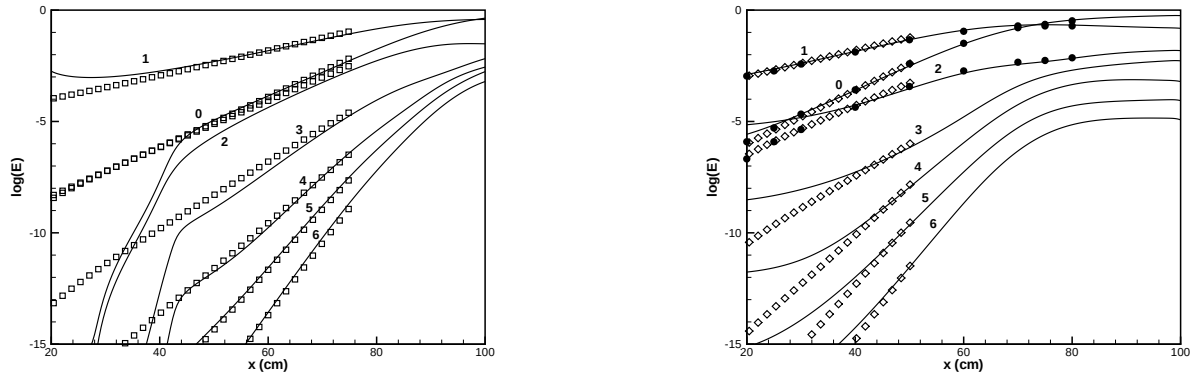

Figure 2: Variation of the energy of each Fourier mode. Fourier modes 0 to 6. Left - Comparison between DNS (solid lines) and PSE results (squares) - Mendonca (2000). Right - Comparison between DNS results (solid lines), PSE results (diamonds) - Mendonca (2000), and results from Li and Malik (1995) (circles).

Figures 3 and 4 show the variation of the streamwise velocity component in the (y, z) plane. The numerical study from Lee and Liu (1992) and the experimental measurements from Swearingen and Blackwelder (1987) are presented for the same streamwise positions along the longitudinal direction. For the two different streamwise positions shown, the development of the mushroom type structures is similar. The numerical results from Lee and Liu (1992) are based on a 2^{nd}-order model, being slightly more dissipative. This behavior can be seen in both figures (Fig. 3 and 4), where the contour lines of streamwise velocity in the head of the mushroom structure goes from $u/\bar{U}_\infty = 0.9$ to $u/\bar{U}_\infty = 0.3$ with the present investigation, being closer to the experimental results.

4.2. Wavelength parameter cases

In this section we present results of simulations performed using three different wavelengths, corresponding to a wavelength parameters for the fundamental Fourier mode Λ_f of 159.1, 450 and 692.6. The two types of

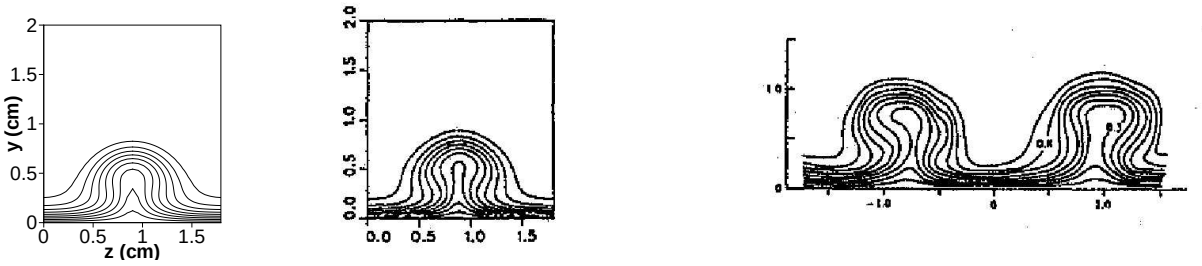

Figure 3: Contour lines of streamwise velocity $u/\bar{U}_\infty$ from 0.1 to 0.9 in increments of 0.1. DNS results-left, other model numerical results -center and experimental results - right. Streamwise position $x = 90$ cm.

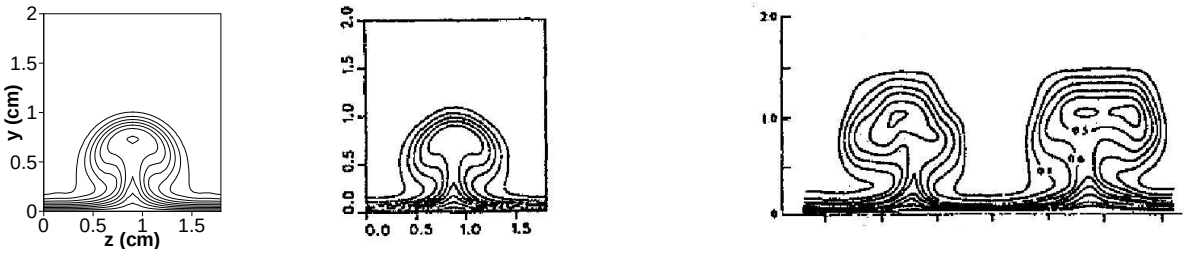

Figure 4: Same as Fig. 3 for streamwise position $x = 100$ cm.

buffer domain near the inflow defined in Sec. 3 are used. Thereafter they are called type 1 and type 2 buffer domain.

The type 2 buffer domain was used because in the introduction of disturbances at the wall using a cosine function with wave number β, in the receptivity region other modes than the fundamental are strongly excited if the corresponding wavenumbers are unstable according to LST. This behavior is not desirable when studying GV of a specific wavelength. The type 2 buffer domain tappers the disturbances of the higher harmonic in the receptivity region, and allow their growth after the fundamental mode starts to propagate as weakly nonlinear GV.

When studying the Boundary-layer receptivity phenomenon due to suction and blowing at the wall it is necessary to use the type 1 buffer domain and let the dominant harmonic grow naturally. The same test case was then run with type 2 buffer domain in order to make comparisons with the weakly nonlinear GV.

In Fig. 5 - left the streamwise development of energy for $\Lambda_f = 692.6$ with type 2 buffer domain is shown. The receptivity region runs approximately from the streamwise position $x = 18$ to $x = 40$ cm. The resulting growth of the disturbance higher harmonics is promoted by the fundamental mode. The use of the type 2 buffer domain reduces the amplitude of the harmonic modes in the receptivity region.

Using the same parameters and a inflow buffer domain of type 1, the resulting streamwise development of the disturbance energy is shown in Fig. 5 - right. When the disturbances are introduced at the wall, both the fundamental and the first harmonic are excited. The first harmonic mode has $\Lambda_f = 244.88$, and therefore, according to LST, a growth rate larger than the fundamental mode. The region of receptivity for the first harmonic is smaller than the corresponding region for the fundamental mode. After the streamwise position of $x = 50$ cm the fundamental and the first harmonic grow with almost the same amplitude until saturation is reached. In Fig. 6 the mushroom pattern of the two simulations are presented at $x = 100$ cm. It can be observed that with type 2 buffer domain, there is only one mushroom structure, and with the type 1 buffer domain, there are 3 mushroom structures in formation. This structure is in agreement with the growth of the energy of the first and higher harmonics, resulting in a shorter wavelength.

A simulation was carried out with the parameter used by Swearingen and Blackwelder (1987) in their experiment. The results are plotted in Figs. 7 - left and 7 - right. The fundamental mode corresponds to a $\Lambda_f = 450$, so its first harmonic has $\Lambda = 159.1$. Here the same behavior observed for $\Lambda_f = 692.6$ can be seen for the fundamental and its first harmonic by comparing the results with the two different types of buffer domain near the inflow. The difference is that, when the fundamental mode saturates, its first harmonic tends to decrease. So, the first harmonic does not have enough energy to change the spanwise pattern. This can be observed by comparing the mushroom structures at the streamwise position of $x = 110$ cm in Fig. 8. A difference between the two results can still be observed, but only one mushroom structure appears. With type 2 buffer domain the downwash region has a weaker velocity gradient at the wall and the stem of the mushroom is narrower. This may have implications in secondary instability.

Figure 9 shows the streamwise development of the disturbance energy in the streamwise direction for type 2 and type 1 buffer domains for simulations with $\Lambda_f = 159.1$. In these cases the first harmonic ($\Lambda = 56.25$) has

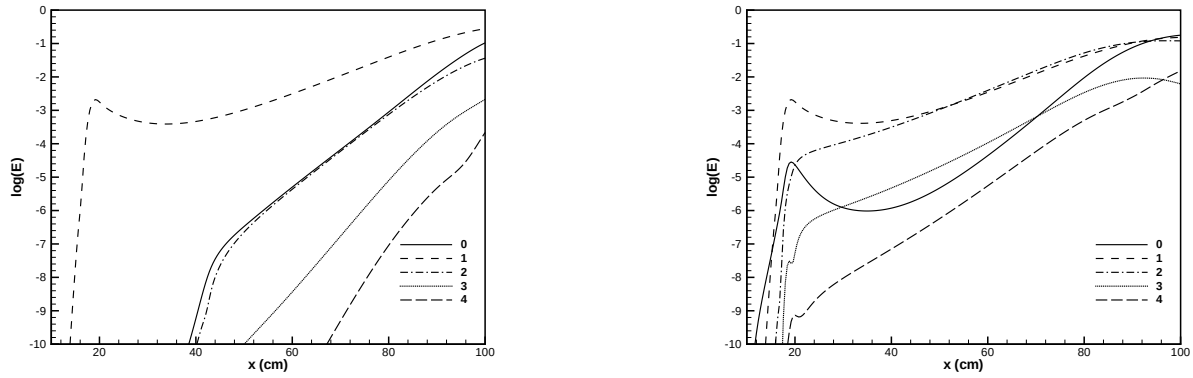

Figure 5: Energy for $\Lambda_f = 692.6$, Fourier modes 0 to 4, Left - type 2 buffer domain, Right - type 1 buffer domain.

Figure 6: Contour lines of streamwise velocity $u/\bar{U}_\infty$ from 0.1 to 0.9 in increments of 0.1. Left - type 2 buffer domain. Right - type 1 buffer domain. $\Lambda_f = 692.6$. Streamwise position $x = 100$ cm.

a very small growth rate. For type 1 buffer domain (Fig. 9 - right), the first harmonic has an initial 'linear' growth, but downstream of the streamwise position $x = 60$ cm the energy behavior of the harmonic modes are almost the same as that of the case with type 2 buffer domain. The mushroom structures for both cases at the streamwise position $x = 100$ cm are shown in Fig. 10. No differences can be observed between these figures.

A last simulation was done with $\Lambda_f = 450$ in which three Fourier modes (1, 2 and 3), with identical amplitudes were excited. The spanwise variation of the normal velocity component at the wall is given by $\cos(\beta_k z) + \cos(2\beta_k z) + \cos(3\beta_k z)$. The resulting streamwise development of the disturbance energy is plotted in Fig. 11 - left. It can be observed that both the fundamental mode (mode 1) $\Lambda_f = 450$ and the first harmonic (mode 2) $\Lambda = 159.1$, have a strong growth, and when mode 2 saturates mode 1 continues to grow. It can also be observed that the Fourier mode 2 grows stronger than mode 1 in the region between streamwise positions $x = 40$ cm and $x = 70$ cm. In Fig. 11 - center and right the mushroom structure is plotted at two streamwise positions, $x = 70$ cm and $x = 110$ cm. At the streamwise position $x = 70$ cm, where mode 2 dominates, two mushroom structures are observed per λ_z. They are modulated so that the one at $z = 0.9$ is largest. At the streamwise position of $x = 110$ cm, the modulated pattern is strongly pronounced. The structure is very different from the typical GV excited single mode. In this case also, the secondary instability will have a different behavior.

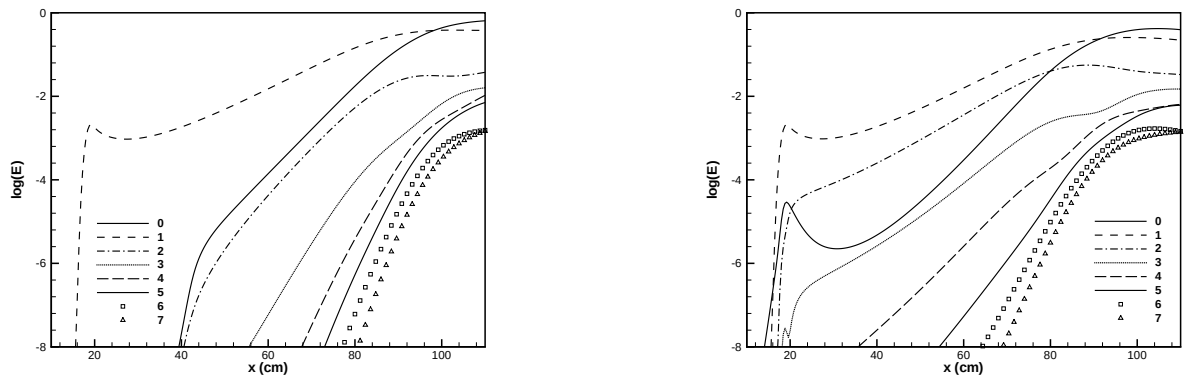

Figure 7: Energy for $\Lambda_f = 450$, Fourier modes 0 to 7, left - type 2 buffer domain, right - type 1 buffer domain.

Figure 8: Contour lines of streamwise velocity $u/\bar{U}_\infty$ from 0.1 to 0.9 in increments of 0.1. Left - type 2 buffer domain. Right - type 1 buffer domain. $\Lambda_f = 450$. Streamwise position $x = 110$ cm.

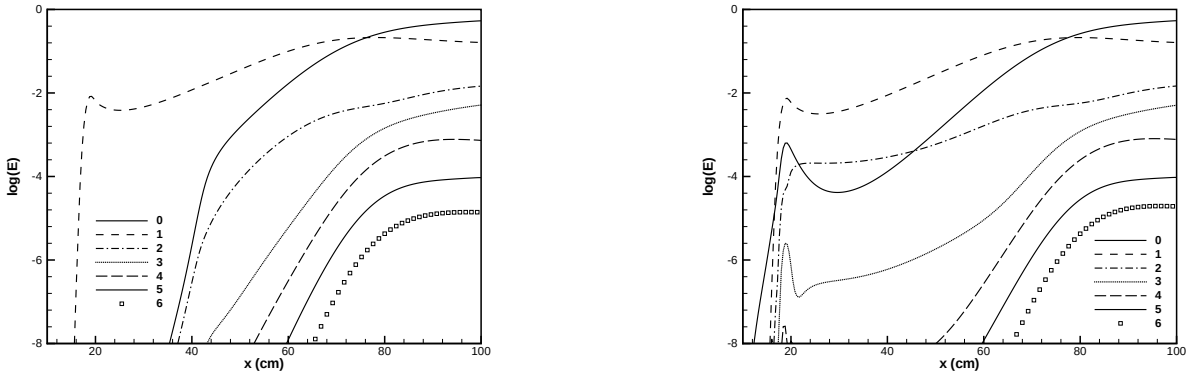

Figure 9: Energy for $\Lambda_f = 159.1$, Fourier modes 0 to 7, left - type 2 buffer domain, right - type 1 buffer domain.

Figure 10: Contour lines of streamwise velocity $u/\bar{U}_\infty$ from 0.1 to 0.9 in increments of 0.1. Left - type 2 buffer domain. Right - type 1 buffer domain. Streamwise position $x = 100$ cm.

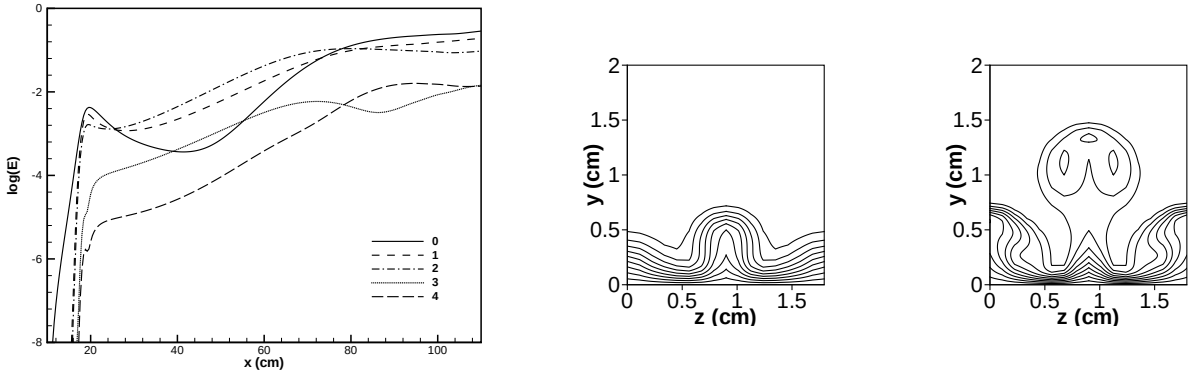

Figure 11: Left - Energy for $\Lambda_f = 450$, type 1 buffer domain, Fourier modes 0 to 4. Middle and left - Contour lines of streamwise velocity $u/\bar{U}_\infty$ from 0.1 to 0.9 in increments of 0.1. Streamwise position $x = 70$ cm - center $x = 110$ cm - right.

5. Conclusions

The paper presents a numerical model based on a high-order compact finite difference scheme to solve the complete Navier-Stokes equations in a direct numerical simulation over concave surfaces. The model was validated by comparing results with three different numerical models (Mendonça, 2000; Li and Malik, 1995; Lee and Liu, 1992). The validation was done by comparing the results with experimental results from Swearingen and Blackwelder (1987).

Görtler vortices generated by disturbances introduced at the wall by suction and blowing in a disturbance strip may have a structure different from the structure observed according to weakly nonlinear theory. This behavior is observed because the suction and blowing region excites different Fourier modes which may be unstable according to LST and a weakly nonlinear theory, having a growth rate higher than the growth rate of the first mode. In previous studies, where Görtler Vortices were seeded by wall roughness and free stream disturbances, this behavior was not observed. The simultaneous growth of the different modes modifies the resulting mushroom pattern. This may have significant consequences for secondary instability, which is strongly dependent on the velocity profiles formed by the vortices.

In order to use the DNS model to study the weakly nonlinear development of Görtler vortices of a specified wavenumber, a damping zone downstream of the suction and blowing strip it was necessary in some cases to eliminate the undesired eigen-modes.

6. Acknowledgments

The first author acknowledges the support received from transition research group of the Institut fur Aerodynamik and Gasdynamik (IAG) from Universität Stuttgart, where he spent 6 months as a visiting scientist.The financial support received from FAPESP is also acknowledged.

7. References

Bottaro, A. and Zebib, A., 1997, Görtler Vortices Promoted by Wall Roughness, "Fluid Dynamics Research", Vol. **19**, pp. 343–362.

Ferziger, J. H. and Peric, M., 1997, "Computational Methods for Fluid Dynamics", Springer, Springer–Verlag.

Guo, Y. and Finlay, W. H., 1994, Wavenumber Selection and Irregularity of Spatially Developing Nonlinear Dean and Görtler Vortices, "J. of Fluid Mechanics", Vol. **264**, pp. 1–40.

Hall, P., 1982, Taylor-Görtler Vortices in Fully Developed or Boundary Layer Flows: linear theory, "J. Fluid Mechanics", Vol. **124**, pp. 475–494.

Kloker, M., Konzelmann, U., and Fasel, H., 1993, Outflow Boundary Conditions for Spatial Navier-Stokes Simulation of Transition Boundary Layer, "AIAA Journal", Vol. 31, No. 4, pp. 620–628.

Lee, K. and Liu, J., 1992, On the Growth of the Mushroomlike Structures in nonlinear Spatially Developing Goertler Vortex Flow, "Physics of Fluids", Vol. **A4**, pp. 95–103.

Lele, S., 1992, Compact Finite Difference Schemes with Spectral-like Resolution, "J. Computational Physics", Vol. **103**, pp. 16–42.

Li, F. and Malik, M. R., 1995, Fundamental and Subharmonic Secondary Instability of Görtler Vortices, "J. Fluid Mechanics", Vol. **297**, pp. 77–100.

Meitz, H. L., 1996, "Numerical Investigation of Suction in a Trasitional Flat-Plate Boundary Layer", PhD thesis, The University of Arizona.

Meitz, H. L. and Fasel, H. F., 2000, A compact-difference scheme for the Navier-Stokes equations in vorticity-velocity formulation., "J. Comp. Phys.", Vol. **157**, pp. 371–403.

Mendonça, M. T., 2000, Parabolized Stability Equations: A Review, "National Congress of Mechanical Engineering - CONEM 2000", Natal - RN.

Myose, R. Y. and Blackwelder, R. F., 1991, Controlling the Spacing of Streamwise Vortices on Concave Walls, "AIAA Journal", Vol. 29, No. 11, pp. 1901–1905.

Souza, L. F., Mendonça, M. T., and Medeiros, M. A. F., 2002a, Assessment of Different Numerical Schemes and Grid Refinement for Hydrodynamic Stability Simulations, "ENCIT 2002, 9th Brazillian Congress of Thermal Engineering and Sciences", Caxambu - MG.

Souza, L. F., Mendonça, M. T., Medeiros, M. A. F., and Kloker, M., 2002b, Three Dimensional Code Validation for Transition Phenomena, "ETT 2002, Third Spring School of Transition and Turbulence", Florianopolis - SC.

Swearingen, J. D. and Blackwelder, R. F., 1987, The Growth and Breakdown of Streamwise Vortices in the Presence of a Wall, "J. Fluid Mechanics", Vol. **182**, pp. 255–290.

Trottenberg, U. and Hackbusch, W., editors, 1986, "Multigrid Methods", Lecture Notes in Mathematics, Springer-Verlag, Koeln-Porz, FRG, 1981: Proceedings.